Determination of Capacities of Eccentric Stiffeners Part 2: Analytical Studies

JAVIER ALVAREZ RODILLA and KEITH KOWALKOWSKI

ABSTRACT

Analytical investigations were performed on column specimens with an effort to evaluate the effective stiffener capacity of eccentric stiffeners when used within moment connections of beams connecting to column flanges. First, analytical models were developed for the experimental column specimens presented in the companion paper Part 1: Experimental Studies (Alvarez Rodilla and Kowalkowski, 2021). These models were utilized to calibrate the finite element methodology and to develop consistent comparisons between the experimental and analytical results.

Finite element models were then developed for larger column sizes more regularly used in practice. In all, 148 models were developed to represent W14×68, W14×120, W14×176, W14×233, W24×131, and W24×229 column specimens. The column models utilized a similar setup to experiments and were subjected to three different loading conditions described as (1) single tension with load pulling away from the column specimen; (2) single compression with load applied toward the column specimen; and (3) double compression with loads applied on both flanges, directly opposite of each other. Parameters also included the unsupported length and stiffener thickness for single compression, the stiffener thickness for double compression, and the weld size/loading plate thickness for single tension. For all test methods and each set of parameters, a group of four column specimens consisted of (1) one modeled without stiffeners, (2) one modeled with concentric stiffeners, (3) one modeled with stiffeners at an eccentricity of 2 in., and (4) one modeled with stiffeners at an eccentricity of 4 in.

The results of the finite element models demonstrate that eccentric stiffeners in practical column sections are more effective in resisting the concentrated load in comparison to smaller column sections. In addition, there were direct trends observed between the magnitude of eccentricity and the elastic stiffness and maximum loads. Utilizing the results, recommendations for determining the effective stiffener capacity of eccentric stiffeners are presented. The recommendations are dependent on the ratio of eccentricity versus flange thickness, or the e/t_f ratio. The research showed that stiffeners at any eccentricity are not effective for a flange thickness less than ½ in. The testing and modeling performed as part of this project studied stiffeners with a maximum eccentricity of 4 in., and therefore, recommendations are limited to this maximum eccentricity.

The analytical investigations also evaluated the limit states associated with concentrated loads with respect to resistance of the column specimen and determined that maximum loads compare well with the limit state of web local crippling and exceeded the limit states of web local yielding and web compression buckling for double compression tests. The results also demonstrate that for an applied tension force, the influence of flange bending should be integrated into the calculations associated with the weld strength in lieu of being evaluated as an independent limit state.

KEYWORDS: steel columns, eccentric stiffeners, moment connections, concentrated loads, flange bending, web compression buckling, web local crippling, web local yielding.

INTRODUCTION AND BACKGROUND

A comprehensive research project was performed at Lawrence Technological University (LTU) to evaluate the influence of stiffener eccentricity on the effective resistance of column members when subjected to concentrated loads as part of moment connections. The study can be extended for the design of stiffeners for other scenarios when wide-flange beams are subjected to concentrated loads. Funding for the research project came from the American Institute of Steel Construction (AISC). For the project, 40 experimental column specimens were tested under concentrated loads without stiffeners, with concentric stiffeners, and with stiffeners at an eccentricity up to 6 in. from the concentrated load. The experimental column specimens were limited to lighter cross sections (W10×19, W10×39, W12×26, and W16×31) due to limitations in the lab facility.

Analytical finite element models were developed to represent the experimental column specimens to calibrate/verify the finite element methodology. Analytical models were developed for larger column sections used more routinely in practice, with additional parameters considered. These column specimens will be referred to as "practical" column specimens herein. This paper discusses the

Javier Alvarez Rodilla, EIT, Graduate Research Scholar, Lawrence Technological University, Southfield, Mich. E-mail: jalvarezr@ltu.edu

Keith Kowalkowski, PhD, PE, SE, Associate Professor, Lawrence Technological University, Southfield, Mich. E-mail: kkowalkow@ltu.edu (corresponding)

Paper No. 2019-16R(2)

analytical studies that followed the experimental investigations. The experimental investigations are presented in the companion paper, Part 1: Experimental Studies (Alvarez Rodilla and Kowalkowski, 2021).

Specifically, this paper describes the methodology used to develop the finite element models. It also shows comparisons between the experimental and analytical results and presents the primary results of the models for practical column specimens. The primary results show relationships between stiffener eccentricity and the effective stiffener capacity. Lastly, the results are compared with the AISC (AISC, 2016) limit states associated with concentrated loads.

The companion paper to this [Part 1: Experimental Studies (Alvarez Rodilla and Kowalkowski, 2021)] provides a thorough overview of background information related to the objectives of the research with a truncated overview provided in this paper. Graham et al. (1959) performed experimental investigations on steel members subjected to concentrated loads with concentric stiffeners and eccentric stiffeners. The primary results of the research showed that transverse stiffeners with a 2-in. eccentricity provide 65% of the strength of an identical concentric transverse stiffener. In addition, it was recommended, "…for design purposes, it would probably be advisable to neglect the resistance of stiffeners having eccentricity greater than 2 in. The required transverse stiffener area, width and thickness can be established by the same criteria as for concentric stiffeners, provided that the strength is reduced linearly from 100 percent at zero eccentricity to 65 percent at 2 in. eccentricity."

Sherbourne and Murthy (1978) performed analytical investigations to study concentrated loads applied to wide-flange sections. The research focused on analyzing the stability of column webs in beam-column moment connections. The author carried out analytical tests on wide-flange sections with concentric and eccentric stiffeners. Eccentric stiffeners were placed at an eccentricity of 25% and 50% of half the column depth. The results showed that the maximum load obtained for the eccentric stiffener cases decreased dramatically compared to the cases with concentric stiffeners, regardless of the column's flange and/or web thickness. At the lower eccentricity, the effectiveness of the stiffeners ranged between 50 and 75% of that for concentric stiffeners. Sherbourne and Murthy also found that the web thickness has a direct influence on the buckling load and behavior of the column.

Norwood (2018) performed analytical research on wide flange sections modeled similar to the experimental tests carried out by Graham et al. (1959) using the finite element method and program ABAQUS (2014). Norwood found that increasing the level of stiffener eccentricity results in a decrease in resistance to concentrated forces. However, the results showed that stiffeners at a 2-in. eccentricity were more effective than the 65% factor provided by Graham et al. The models consisted of four-noded linear shell elements with reduced integration as well as a cyclic nonlinear kinematic material hardening based on the plastic strain behavior of A572 Gr. 50 steel. As discussed in the next section, the material properties utilized were similar to those used for the finite element models presented in this paper. However, the choice of element type and the analysis method are notably dissimilar.

OVERVIEW OF FINITE ELEMENT MODELS

Model Parts and Element Types

Finite element models included the column specimens themselves, stiffeners at or near mid-length, bearing stiffeners near the supports, and loading plates. Loading plates include the top loading plate for all test methods and the bottom reaction plates for double compression tests. Figure 1 provides a screenshot showing an isometric view of the finite element model of a W14×68 double compression column specimen with concentric stiffeners (or mid-length and in line with applied load). This finite element model does not have bearing stiffeners. However, for single tension and single compression models, bearing stiffeners were modeled in the same way as mid-length stiffeners.

Models of steel plates utilized either solid elements or shell elements. Models for wide flange column specimens utilized solid elements due to the presence and significance of the fillet region of the column specimens. Solid elements were also used for modeling the loading plates and welds. Initially, type C3D8I elements were used for calibration of the models, which are eight-node, three-dimensional continuum elements with three degrees of freedom per node and enhanced by incompatible modes to improve bending behavior (ABAQUS, 2014). However, for some practical column specimens, the finite element models had issues converging to a solution due to severe distortions of the elements. Therefore, in all models of practical column specimens, the column specimens and loading plates were modeled with type C3D8R elements, which is an eight-node linear brick, reduced integration with hourglass control element (ABAQUS, 2014). Studies in Kowalkowski and Alvarez Rodilla (2019) showed negligible differences in the results of column specimens modeled using both types of elements. High local deformations near the application of the concentrated load required finer meshes to be used in these areas. Conversely, coarser meshes were utilized away from the concentrated loads and near supports where local deformations are less significant. Mesh sensitivity studies were performed prior to initiating the experimental investigations. As shown in this paper, because the analytical

results compare favorably to experimental results with respect to maximum loads, it is assumed that the element mesh was adequate.

Stiffeners were modeled utilizing four-node linear shell elements of type S4 (ABAQUS, 2014). These elements are general-purpose shell elements and have six deformation degrees of freedom per node.

For all compression tests, the loading plates were modeled by direct attachment to the column specimens by sharing the nodes. Modeling of welds between the loading plates and the top flange of the column specimen was deemed critical for all tension models. Welds were modeled with C3D8 elements (ABAQUS, 2014). These elements are three-dimensional continuum elements with three degrees of freedom per node. The elements were arranged together in a triangular pattern with a slight gap at the apex. In order to provide compatibility between the welds and the connecting flange and plate, each node on the welds that connect to the plate elements was constrained (slaved) to a node on the plate elements, therefore ensuring the displacements in all three directions (DOF 1, 2, and 3 as shown in Figure 4) were the same. A screenshot of a finite element model at the weld location is shown in Figure 2.

Material Properties

Calibration of finite element models for the experimental column specimens utilized material properties determined from uniaxial tension tests performed per ASTM E8/E8M-09 (ASTM, 2009) on samples fabricated from the webs and flanges of the column specimens. Practical column specimen models utilized minimum material properties defined in the AISC *Steel Construction Manual* (AISC, 2017) for ASTM A992 steel. These properties include a minimum yield stress of 50 ksi, a minimum ultimate stress of 65 ksi,

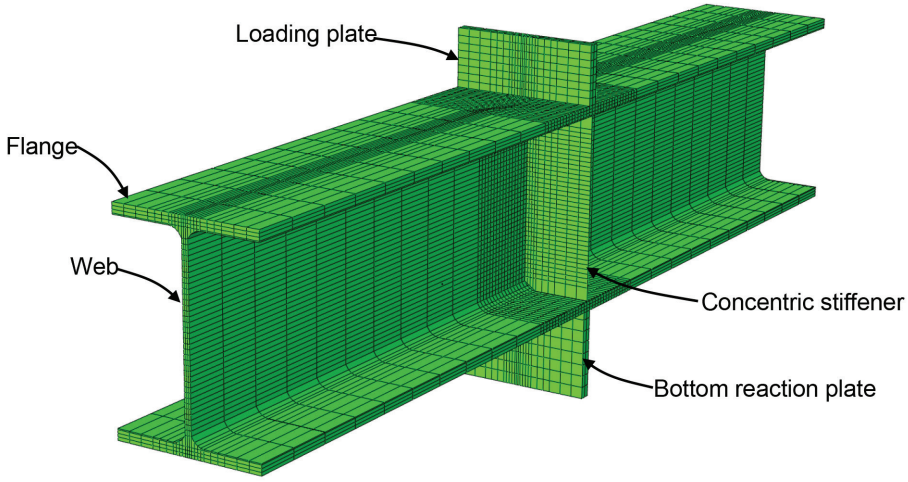

Fig. 1. Isometric view of finite element model of W14×68 double compression specimen.

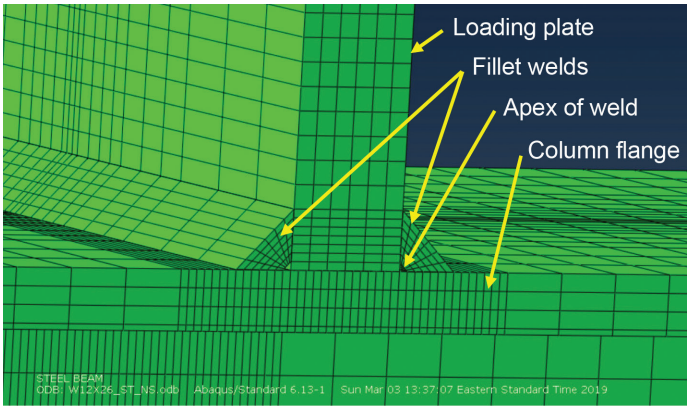

Fig. 2. Finite element model of a single tension test at the weld.

and an elastic modulus of 29,000 ksi. Results from uniaxial tension tests performed on samples fabricated from the column specimens formed the basis of stress-strain relationships used in modeling. Figure 3 demonstrates how the engineering stress-strain curves derived from samples taken from the column specimens were modified to develop similar engineering stress-strain curves with the minimum properties specified for A992 steel.

During the experimental investigations, uniaxial tension tests on samples fabricated from stiffener material revealed that some of the material met the requirements for both ASTM A36 and ASTM A572 material and was thus dual-certified material. Due to uncertainties associated with the stiffener material and properties of stiffeners used in practice, all stiffeners were modeled with the same material properties as the column specimens in both the calibration studies and the practical column specimen studies. Some differences are anticipated in results if different material properties are used. However, in most analytical models with mid-length stiffeners, the stiffeners buckled, which is less dependent on the strength of the material and more dependent on the elastic modulus, which is relatively constant for various steel grades.

Loading plates in finite element models of practical column specimens were modeled as elastic only with an elastic modulus of 29,000 ksi. The elastic behavior allowed the loading plates to deform as the column specimen flanges and/or welds deformed but prevented them from developing significant inelastic deformations and thus controlling the failure mode associated with the finite element models.

Material properties of the weld were deemed critical for all single tension models. The basis of this assertion comes from the experimental studies showing the maximum load is generally governed by non-uniform stresses that develop in the welds. Several researchers have reported the yield and ultimate stress of weld materials. For instance, Bowman and Quinn (1994) and Kartal et al. (2007) presented weld material test results. The nonlinear stress-strain curve and the ultimate stress of the weld material (82.4 ksi) was based on the experimental results by Kartal et al. Additional information regarding the literature review on weld material properties and an idealization used in the analytical models for the nonlinear stress-strain curve is found in Kowalkowski and Alvarez Rodilla (2019).

Boundary Conditions and Loading

The connection between the stiffeners and the column section (shell-to-solid connection) was modeled by extending the elements of the stiffeners one-element thickness into the solid elements and connecting the nodes on the stiffeners to the intersecting nodes within the solid elements.

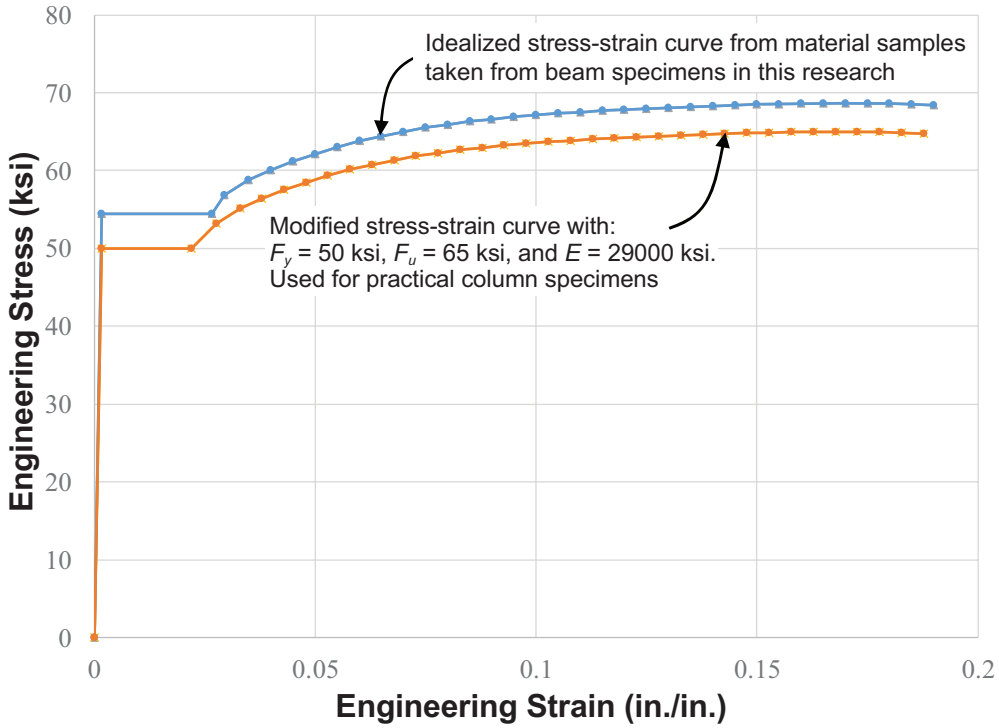

Fig. 3. Idealized stress-strain curves used for analytical studies.

To relate to the experimental tests presented in Part 1: Experimental Studies (Alvarez Rodilla and Kowalkowski, 2021), all column specimens were assumed to react against roller supports. For the compression models, the supports were located 6 in. from the ends and in contact with the bottom nodes of the bottom flanges. Roller supports were modeled in contact with the top flange in tension models. In the analytical models, the nodes along the width of the flange at these locations were fixed vertically (DOF 2, see Figure 4) to simulate the boundary conditions.

The center nodes on the loading plates and through the depth were fixed in the transverse direction (DOF 3) to avoid elastic buckling under higher loads. Loading was applied by specifying an incremental displacement using the *BOUNDARY option (ABAQUS, 2014). The center node on the top of the loading plate was modeled as the control node to specify the displacement. Other nodes on the top surface of the top plate were slaved to the control node in the vertical direction (DOF 2). The top of the top plate was also fixed in the other transverse direction (DOF 1). Figure 4 shows an isometric view of a finite element model of a W10×39 column specimen and graphics associated with the boundary conditions.

In the experimental investigations, the double compression tests revealed that fewer local deformations occurred near the bottom flange of the column specimen as opposed to the top flange of the column specimen, and the end of the column specimen rotated slightly about the *x*-axis of the cross section (DOF 1 per Figure 4) as local deformations progressed. These observations suggest the load did not completely transfer from the upper loading plate to the bottom reaction plate. Instead, some of the force transfers to the end supports. During the calibration phase with the experimental column specimens, the bottom of the bottom plate was fixed in all three directions (DOF 1, 2, and 3) because loading was only applied from the actuator on the top. However, for the practical column specimens, the bottom plate was constrained to have the same displacement as the top loading plate but in opposite directions, simulating a true through force and equal local deformations on each side of the column flange, similar to the condition in an actual moment connection with equal compression forces on either side of the column.

Analysis Procedure

Multiple analysis procedures were evaluated to simulate and analyze the deformations and stresses that develop in the finite element models. In all cases, loads were applied in increments to observe the load-displacement results and behavior. For all the single tension models, a general static analysis was performed using the *STATIC analysis procedure available in ABAQUS. For compression models, first, an eigenvalue analysis was carried out in ABAQUS to simulate a buckled shape. In the eigenvalue analysis, the finite element software identifies multiple buckling or mode shapes for the column specimen. The eigenvalue analysis in ABAQUS scales the maximum resultant displacement at any point to a maximum value of 1 (in this case, this would represent 1 in. because in. were assumed in the development of all models). Following the eigenvalue analysis, a geometric imperfection was specified in ABAQUS, which represents a small percentage of the buckled shape determined from the eigenvalue analysis. After specifying the

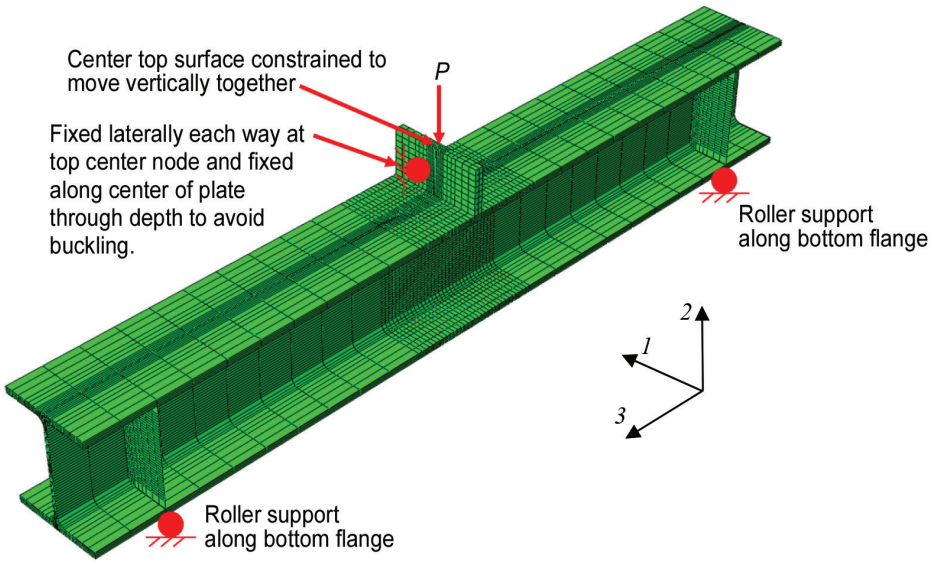

Fig. 4. Isometric view of finite element model showing boundary conditions.

Table 1. Analytical Test Matrix for Experimental Column Specimens	
Column Specimen Nomenclature	**Column Specimen Nomenclature**
W10×19 DC-E0	W12×26 SC-E0
W10×19 DC-NA	W12×26 SC-NA
W12×26 DC-E0	W12×26 SC-E4
W12×26 DC-NA	W12×26 ST-E0
W12×26 DC-E4	W12×26 ST-E4
W16×31 DC-NA	W16×31 ST-E0
W10×39 SC-E0	W16×31 ST-NA
W10×39 SC-NA	

imperfection, a static-stress analysis was performed using the *STATIC RIKS option. The *STATIC RIKS analysis is generally used to predict geometrically nonlinear collapse of a structure (ABAQUS, 2014). This allowed the models to buckle by modes of web local crippling, web compression buckling, and stiffener buckling and to study the post-buckling behavior. The analyses performed for each type of model is demonstrated in Figure 5.

CALIBRATION STUDIES FOR FINITE ELEMENT MODELS

Analytical investigations using the experimental column specimens were performed to calibrate the finite element modeling techniques. Finite element models were developed for all four experimental column specimen sizes (W16×31, W12×26, W10×19, and W10×39). Fifteen finite element models were used for this study. Table 1 shows the full analytical test matrix for the experimental column specimens. The nomenclature used for each column specimen includes the column specimen size, the test method, and the stiffener condition. For the test method, DC refers to double compression, SC refers to single compression and ST refers to single tension. For the stiffener condition, NA indicates a test without mid-length stiffeners, E0 refers to a column specimen with concentric stiffeners, and E4 refers to a column specimen with stiffeners at an eccentricity of 4 in.

The calibration studies identified that the analytical models for column specimens compared well with the experimental results when using a geometric imperfection during the *STATIC RIKS analysis (ABAQUS, 2014) for compression tests. Different magnitudes of geometric imperfections were evaluated in the calibration studies. Imperfections exist in any steel cross section as no member is fabricated perfectly. However, accurate measurements of such imperfection were not considered during the experimental phase of the project. A magnitude of imperfection

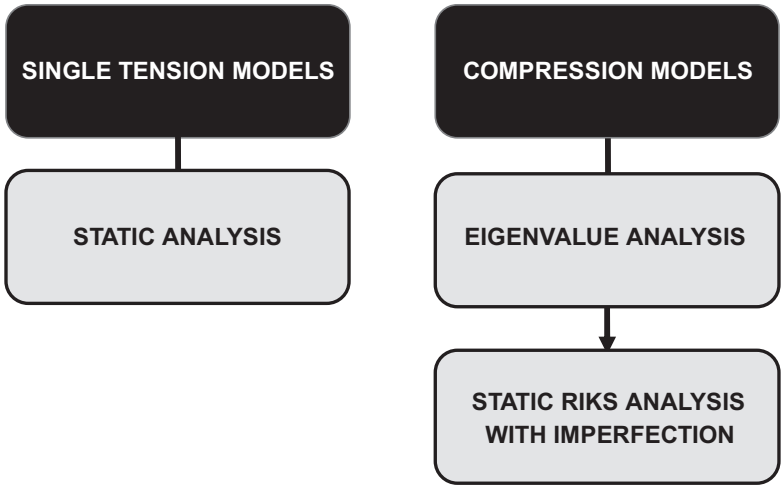

Fig. 5. Analysis procedure for different types of analytical models.

equal to 0.001% (maximum out-of-plane deformation = 0.00001 in.) of the displacement of the buckled shape from the eigenvalue analysis provided the best analytical results in comparison to the experimental results for most column specimens. For instance, Figure 6 shows the load-displacement results for finite element models of a W10×39 column specimen tested in single compression and without stiffeners (W10×29 SC-NA) and for various imperfections compared to the experimental results. There are discrepancies between the analytical and experimental results with respect to the elastic stiffness. The research team could not identify any flaws with the analytical models to account for this. The analytical results were compared to theoretical predictions in the elastic range only, and analytical and theoretical studies discussed in Kowalkowski and Alvarez Rodilla (2019) indicated that the finite element models are accurately predicting the elastic stiffness and displacement results. Therefore, discrepancies were due to flaws in the experimental stroke displacement of the actuator. The maximum loads and behavior when web crippling occurred compared favorably for all compression models when utilizing a 0.001% imperfection. Figure 6 thus helps support the justification for the use of a 0.001% imperfection in the model.

Studies were performed for all compression tests listed in Table 1 in a similar way to those done to generate Figure 6. The analytical results were in line with one of the primary conclusions discussed in Part 1: Experimental Studies (Alvarez Rodilla and Kowalkowski, 2021) in that, for these column sizes, eccentric stiffeners at an eccentricity of 4 in. have a small influence on the maximum load obtained for the column specimen and web crippling still occurred.

It was critical for the single tension tests to calibrate when weld fracture occurred in the elements utilized for modeling welds. Weld failure was assumed to occur when the von Mises stress exceeded the ultimate stress, specified as 82.4 ksi (discussed previously). Also, plastic strains were checked in the models and failure was defined as equivalent plastic strains exceeding 0.2 in./in. For all finite element models of single tension tests, the loads corresponding to when these two events occurred compared favorably to the maximum loads obtained in the experimental results when weld fracture occurred. In the analytical models of practical column specimens, failure was always assumed to occur when the von Mises stress exceeded the ultimate stress of 82.4 ksi. The equivalent plastic strain was not used.

ANALYTICAL TEST MATRIX FOR PRACTICAL COLUMN SPECIMENS

After validating the finite element methodology, the practical column specimens were modeled and evaluated. A summary of the analytical test matrix for the practical column specimens analyzed is provided in Table 2. The nomenclature in Table 2 represents an "analysis set" of four specimens. For each analysis set, (1) one model was analyzed with no stiffeners near the concentrated load, (2) one was analyzed with concentric stiffeners, (3) one was analyzed

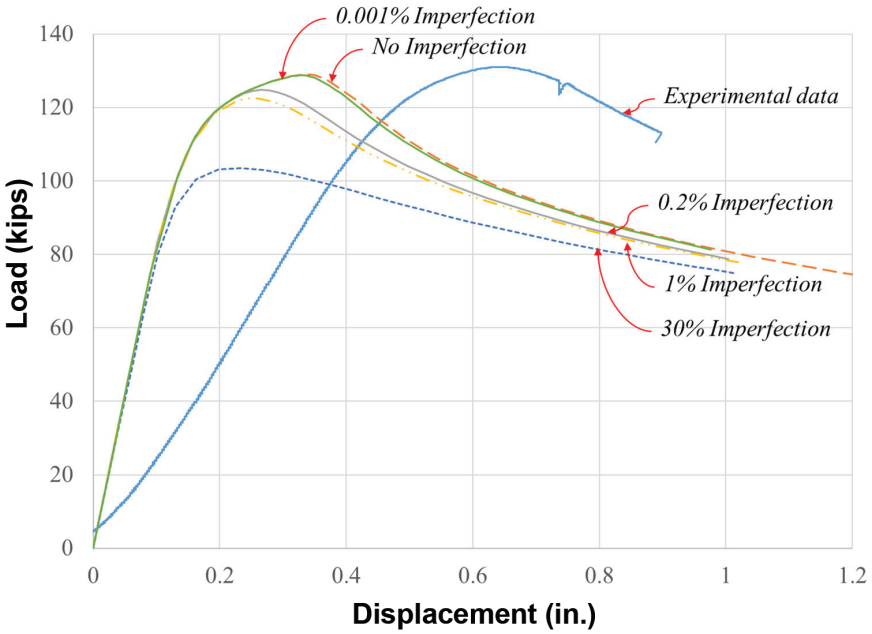

Fig. 6. Load-displacement comparison between experimental and analytical results for the W10×39 SC-NA column specimen.

Table 2. Analytical Test Matrix for Practical Column Sizes						
Nomenclature	**Test Method**	**Column Size**	**Stiffener t_s (in.)**	**Unsupported Length (ft)**	**Plate t (in.)**	**Weld (in.)**
W24×131 SC-⅜	Single Compression	W24×131	⅜	5	1	NA
W24×22 SC-⅜		W24×229	⅜	5	1	NA
W14×68 SC-⅜		W14×68	⅜	5	1	NA
W14×120 SC-⅜		W14×120	⅜	5	1	NA
W14×176 SC-⅜		W14×176	⅜	5	1	NA
W14×233 SC-⅜		W14×233	⅜	5	1	NA
W24×229 SC-¾		W24×229	¾	5	1	NA
W14×233 SC-¾		W14×233	¾	5	1	NA
W14×233 SC-¾(2)		W14×233	¾	**3.5**	1	NA
W24×131 DC-⅜	Double Compression	W24×131	⅜	NA	1	NA
W24×229 DC-⅜		W24×229	⅜	NA	1	NA
W14×68 DC-⅜		W14×68	⅜	NA	1	NA
W14×120 DC-⅜		W14×120	⅜	NA	1	NA
W14×176 DC-⅜		W14×176	⅜	NA	1	NA
W14×233 DC-⅜		W14×233	⅜	NA	1	NA
W24×131 DC-¾		W24×131	¾	NA	1	NA
W24×229 DC-¾		W24×229	¾	NA	1	NA
W14×68 DC-¾		W14×68	¾	NA	1	NA
W14×120 DC-¾		W14×120	¾	NA	1	NA
W14×176 DC-¾		W14×176	¾	NA	1	NA
W14×233 DC-¾		W14×233	¾	NA	1	NA
W24×131 ST-¼	Single Tension	W24×131	⅜	5	¾	¼
W24×229 ST-¼		W24×229	⅜	5	¾	¼
W14×68 ST-¼		W14×68	⅜	5	¾	¼
W14×120 ST-¼		W14×120	⅜	5	¾	¼
W14×176 ST-¼		W14×176	⅜	5	¾	¼
W14×233 ST-¼		W14×233	⅜	5	¾	¼
W24×131 ST-9⁄16		W24×131	⅜	5	1½	9⁄16
W24×22 ST-9⁄16		W24×229	⅜	5	1½	9⁄16
W14×68 ST-9⁄16		W14×68	⅜	5	1½	9⁄16
W14×120 ST-9⁄16		W14×120	⅜	5	1½	9⁄16
W14×176 ST-9⁄16		W14×176	⅜	5	1½	9⁄16
W14×233 ST-9⁄16		W14×233	⅜	5	1½	9⁄16
W24×131 ST-⅞		W24×131	⅜	5	2¼	⅞
W24×229 ST-⅞		W24×229	⅜	5	2¼	⅞
W14×68 ST-⅞		W14×68	⅜	5	2¼	⅞
W14×120 ST-⅞		W14×120	⅜	5	2¼	⅞
W14×176 ST-⅞		W14×176	⅜	5	2¼	⅞
W14×233 ST-⅞		W14×233	⅜	5	2¼	⅞

with stiffeners at a 2 in. eccentricity from the concentrated load, and (4) one was analyzed with stiffeners at a 4 in. eccentricity from the concentrated load. For each analysis set, Table 2 indicates the test type, the column size, the thickness of the stiffener, the unsupported length (one additional analysis set was performed with an unsupported length of 3.5 ft in lieu of 5 ft), the thickness of the loading plate(s), and the weld size used in the models for single tension tests.

The nomenclature of each analysis set includes the column size and the test method (SC for single compression, DC for double compression, and ST for single tension) along with an additional parameter, which depends on the test method. For the single tension tests, the additional parameter represents the weld thickness from the loading plate to the top flange of the column specimens. For double compression and single compression tests, the additional parameter represents the stiffener thickness. The nomenclature used for an individual model includes the nomenclature shown in Table 2 along with a representation of the stiffener eccentricity condition (NA for no stiffener, E0 for concentric stiffener, E2 for a 2-in. eccentricity, and E4 for a 4-in. eccentricity).

Table 2 shows the six practical column sizes selected for analytical investigations, including four W14 sizes. An increase in the flange thickness, decrease in the slenderness of the flange ($b_f/2t_f$), and decrease in the slenderness of the web (h/t_w) occur as the size (with respect to weight) of the W14 increases except for flange slenderness between the W14×120 and W14×68. This general trend in the W14 sections reflect an increase of "stockiness" for the specimens as their weight increases. Additionally, two W24 sections were modeled to represent shapes more commonly used in seismic areas or drift susceptible regions.

For the single tension tests, weld sizes of ¼ in., 9⁄16 in., and ⅞ in. were selected for the test matrix. Various weld sizes were analyzed since weld sizes proved to be an important testing parameter. Each weld size utilized a different loading plate thickness to ensure failure did not occur in the base metal before the weld.

Initially, the stiffener thickness was not thought of as a crucial parameter in the analytical studies because the primary focus of the research was to identify the change in effective capacity for eccentric stiffeners in lieu of concentric stiffeners, and it was believed that similar results would be obtained in identifying the percent changes, regardless of the stiffener thickness. There were no specific design loads, and therefore, the stiffeners were not designed using typical design equations. AISC *Specification* Section J10.8 (AISC, 2016) indicates that the thickness of the stiffener plate shall not be less than one-half the thickness of the loading plate. Because the loading plate was initially ¾ in. thick, a minimum stiffener thickness of ⅜ in. was initially selected for all models, which also matched the thickness of stiffeners used experimentally as described in Part 1: Experimental Studies (Alvarez Rodilla and Kowalkowski, 2021). However, results of some compression tests revealed that thin stiffeners might be more susceptible to buckling if concentric as opposed to eccentric. The results utilizing ⅜-in. stiffeners provided valuable results for some models but did not provide valuable results for all conditions, particularly when used in double compression tests for "stockier" members. An alternate stiffener size of ¾ in. was chosen to evaluate/validate the results and conclusions derived using ⅜-in. stiffeners.

ANALYTICAL FINITE ELEMENT BEHAVIOR

The following various screenshots from ABAQUS (2014) are provided to visualize observed model behavior herein.

Single Compression Models

All single compression column specimens *without stiffeners* reached their capacity when web crippling occurred within the web at a localized area under the applied load. Depending on the column size, significant yielding was also observed in the finite element model before crippling and contributed significantly to the mode of failure. Therefore, inelastic localized web crippling best describes the observed failure modes.

Generally, the maximum load for analytical column specimens *with concentric stiffeners* occurred when buckling took place in the stiffeners. In some cases, buckling of the stiffener was instantaneous and caused a sudden decrease in load (elastic stiffener buckling). Stiffener buckling for other column specimens occurred more gradually and after a significant amount of yielding occurred in the column specimen. The mode of stiffener buckling was dependent on the stiffener thickness and column size.

For modeled column specimens *with eccentric stiffeners*, the maximum load occurred when a combination of web local crippling and stiffener buckling/bending occurred. In some cases, significant yielding occurred in the stiffeners and the column specimen before reaching a maximum load and suggests that with practical column sizes, the stiffeners are more effective in sharing the concentrated load.

Figure 7 shows a screenshot of the W14×68 analytical model without stiffeners (W14×68 SC-NA) after web crippling occurred within the web. The contours represent the resultant magnitude of displacement at each point in the column specimen and demonstrate the out-of-plane displacement of the web with the vertical displacement of the loading plate. As soon as out-of-plane displacements occurred within the web, the load started to decrease gradually, indicating a buckling mode of failure occurred.

Figure 8 shows a screenshot of a W14×233 analytical model without stiffeners (W14×233 SC-NA) after web crippling occurred. Out-of-plane displacement is more concentrated toward the top flange for this column size. Also, the finite element model demonstrated more yielding prior to web crippling.

Figure 9 shows a finite element model for a W24×131 analytical model with concentric stiffeners (W24×131 SC-E0-⅜) and demonstrates that stiffener buckling eventually occurred directly under the concentrated load. The contours represent the von Mises stress magnitude at each point in the column specimen. Similarly, Figure 10 shows a finite element model of a W24×131 column specimen with stiffeners at an eccentricity of 4 in. (W24×131 SC-E4-⅜) and demonstrates how the stiffeners bend/buckle in combination with web local crippling.

Double Compression Tests

All double compression column specimens *without stiffeners* reached their capacity when sudden web compression buckling took place. The buckled shape of the web appeared as either one half-sine wave or two half-sine waves as shown in Figure 11 for a W14×68 column specimen (W14×68 DC-NA) and Figure 12 for a W14×120 column specimen (W14×120 DC-NA). Similar to single compression tests, for column sections with stockier webs, more yielding occurred before inelastic web compression buckling, and the out-of-plane deformation was not as significant as for members with thinner webs.

The maximum load for modeled column specimens *with concentric stiffeners* always took place when buckling occurred in the stiffeners. This buckling caused a sudden decrease in load for a given displacement. The results showed that with heavier (or stockier) column sections, ⅜-in. concentric stiffeners were more detrimental to the column specimen than the no-stiffener condition because buckling occurred suddenly before the web could properly distribute the load, as explained in more detail in Kowalkowski and Alvarez Rodilla (2019). Utilizing ¾-in. stiffeners always aided the capacity of the column specimen.

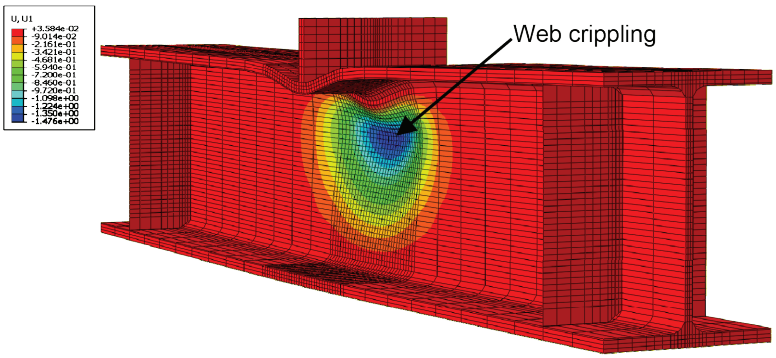

Fig. 7. Web local crippling that occurred in W14×68 SC-NA.

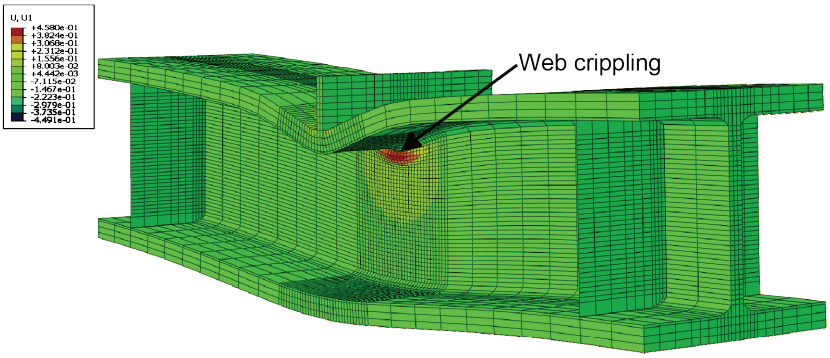

Fig. 8. Localized web local crippling that occurred in W14×233 SC-NA.

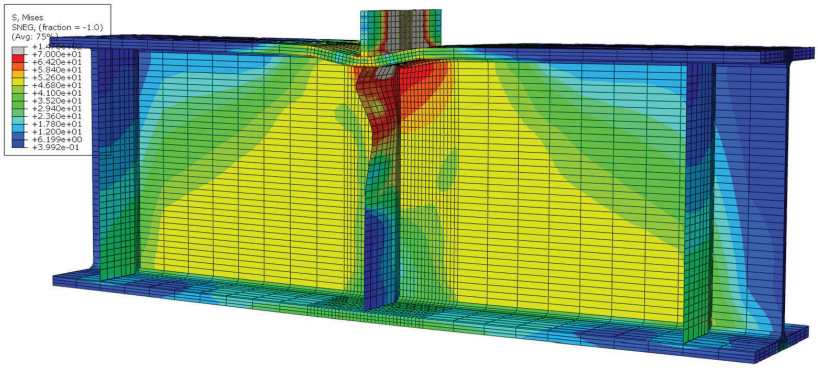

Fig. 9. Stiffener buckling that occurred for W24×131 SC-E0-⅜ (⅜-in. stiffeners).

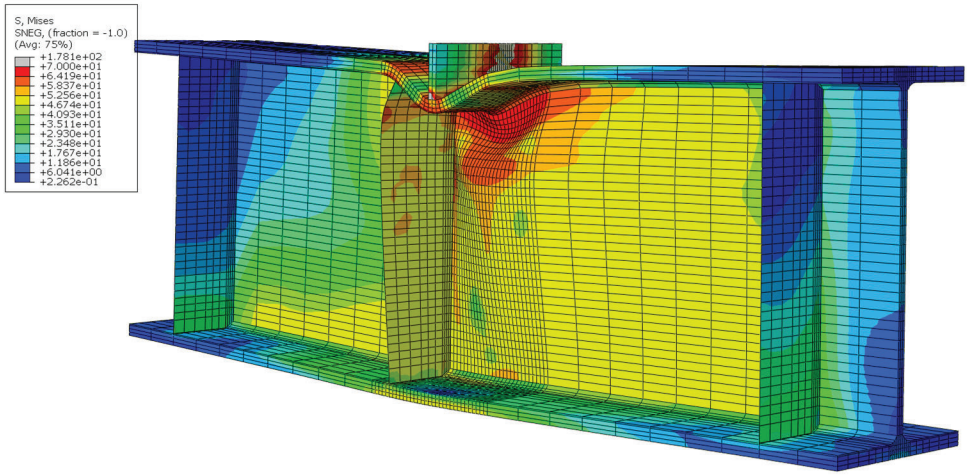

Fig. 10. Web local crippling combined with stiffener bending for W24×131 SC-E4-⅜.

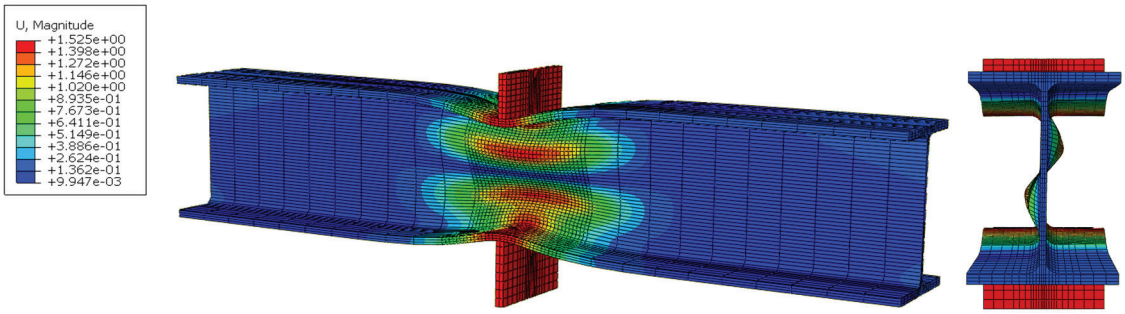

Fig. 11. Web compression buckling for column specimen W14×68 DC-NA.

Further, in some cases, yielding occurred in the stiffeners before stiffener buckling. Figure 13 shows a screenshot of a W14×131 model where the buckling of a ¾-in. concentric stiffener occurred.

For modeled column specimens *with eccentric stiffeners*, a combination of failure modes associated with the column specimen itself sometimes combined with bending of the stiffener generally controlled achieved capacity. In some cases, it appeared that eccentric stiffeners were more beneficial than concentric stiffeners since "sudden" buckling did not occur. Instead, the stiffeners started to develop curvature as deformations developed in the column specimen and still adequately braced the web from compression buckling. Figure 14 shows an example of a W24×131 column specimen modeled with ¾-in. stiffeners at an eccentricity of 4 in. (W24×131 DC-E4-¾). In this example, buckling of the web appeared to occur first as the limited load got transferred into the stiffeners at this eccentricity. As further deformations developed, more load was carried by the stiffeners until the stiffener buckled. This observed behavior is annotated on Figure 15, which shows the load-displacement results for all four modeled W24×131 column specimens together. As shown in Figure 15, the stiffeners at a 2-in. eccentricity were able to carry significant load prior to stiffener buckling. In this particular case, the maximum loads are very similar for the condition with concentric stiffeners and with stiffeners at a 2-in. eccentricity.

Single Tension Tests

The maximum load for the single tension finite element models was assumed to occur when the welds connecting the loading plate to the top flange reached the ultimate stress of 82.4 ksi at some location along the length of the weld. Calibration and verification of this process using experimental results and finite element models of the experimental column specimens is further described in Kowalkowski and Alvarez Rodilla (2019) and explained earlier in this paper. Each model was visually inspected in ABAQUS (2014) to identify when this occurs using the von Mises stresses distribution and setting the maximum limit to 82.4 ksi. Figure 16 shows a W24×131 column specimen

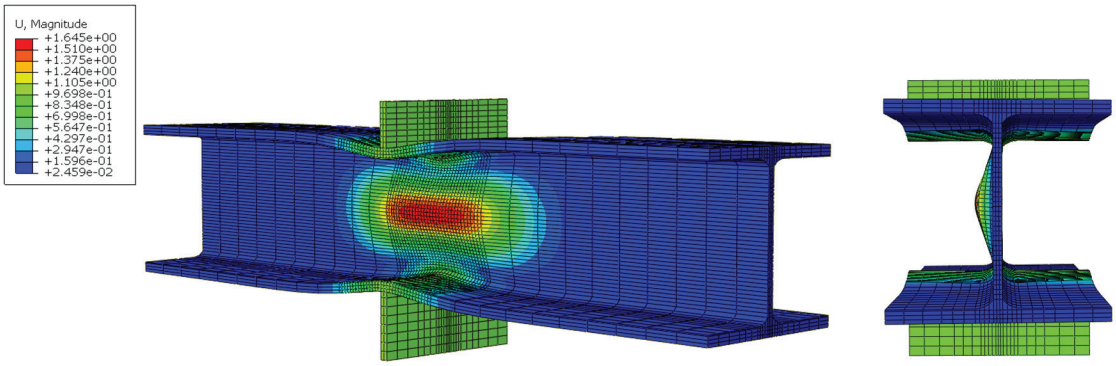

Fig. 12. Web compression buckling for column specimen W14×120 DC-NA.

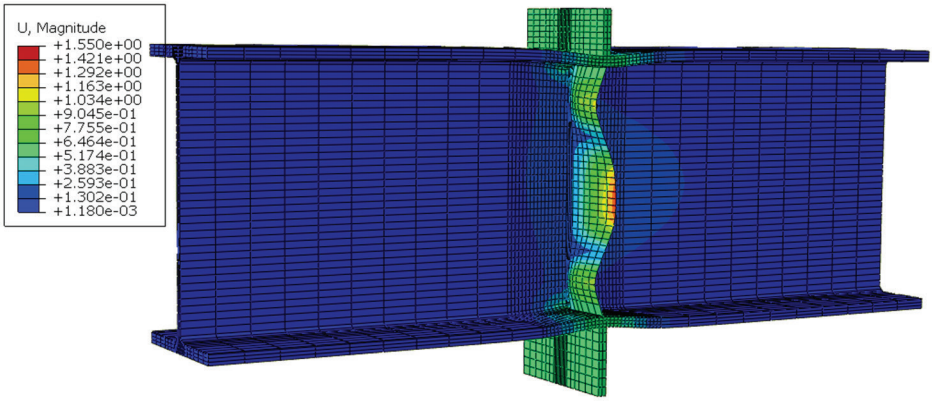

Fig. 13. Stiffener buckling that occurred for W24×131-DC-E0-¾.

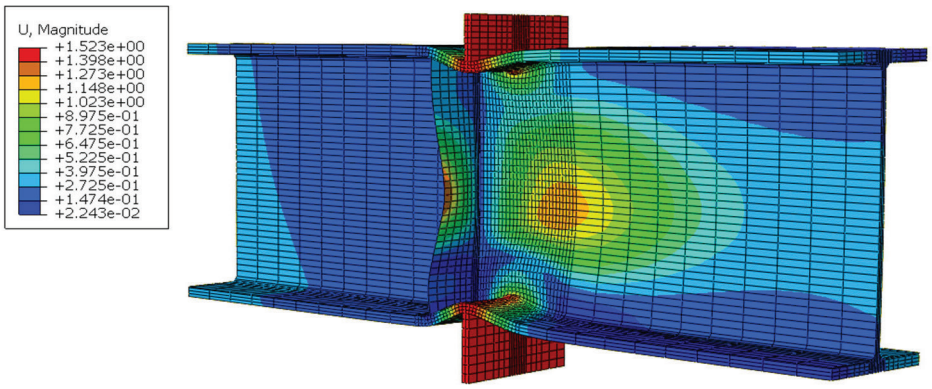

Fig. 14. Web compression buckling with stiffener buckling for W24×131 DC-E4-¾.

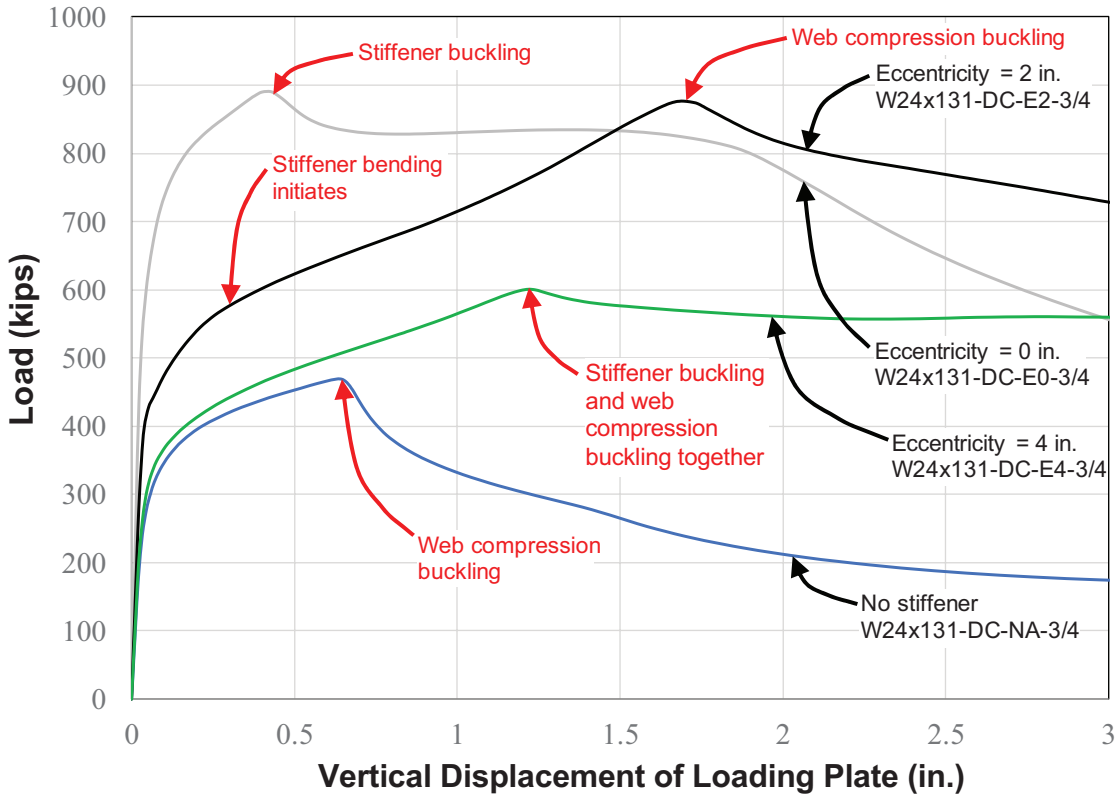

Fig. 15. Load-displacement results of W24×131 DC-¾ column specimens.

modeled with ¼-in. welds. Failure was assumed to occur in the top of the weld where it connects to the loading plate. Figure 17 shows a W24×131 column specimen modeled with ⅞-in. welds, and failure was assumed to occur at the bottom of the welds, where they connect to the column specimen flange. Note that in these figures, anything gray in the finite element models indicated an area where the Von Mises stress exceeded 82.4 ksi.

All column specimens modeled with ¼-in. welds reached an assumed failure load with a stress contour pattern similar to that shown in Figure 16. Also, larger column sections (e.g., W14×233 and W24×229) always reached an assumed failure load with contours similar to that shown in Figure 16, regardless of weld size. In limited conditions, the stress contours never exceeded the ultimate stress and, therefore, never demonstrated a failure in the weld. Rather, the column specimens exhibited significant displacements, and capacity was governed by the shear and flexural stresses that developed in the column specimen. This only occurred when ⅞-in. welds were modeled and stiffeners were at an eccentricity of 0 or 2 in.

In general, stress concentrations develop near the center of the weld along the length due to bending that occurred in the flanges. Near the center of the weld, the column section is stiffened by the fillet region and web adjacent to it, whereas near the edges of the weld, stiffness decreases because there is nothing adjacent below the flange. Therefore, less stress develops in the welds since the flanges locally displace vertically under the applied load. As the thickness of the flange increases and the slenderness of the flange decreases, the flange is less susceptible to develop local relative deformations. When stiffeners are present and adjacent to the weld, a load path exists to transfer force directly into the stiffeners, and the flanges are less prone to bend, allowing more force to develop at the connection since more uniform stresses develop in the weld.

For the single tension models, the influence of stiffener eccentricity on the maximum loads when failure of the welds was assumed to occur varied significantly for the different weld sizes. However, in all comparisons, as weld size increased and stiffener eccentricity decreased, the maximum load obtained when failure was assumed to occur

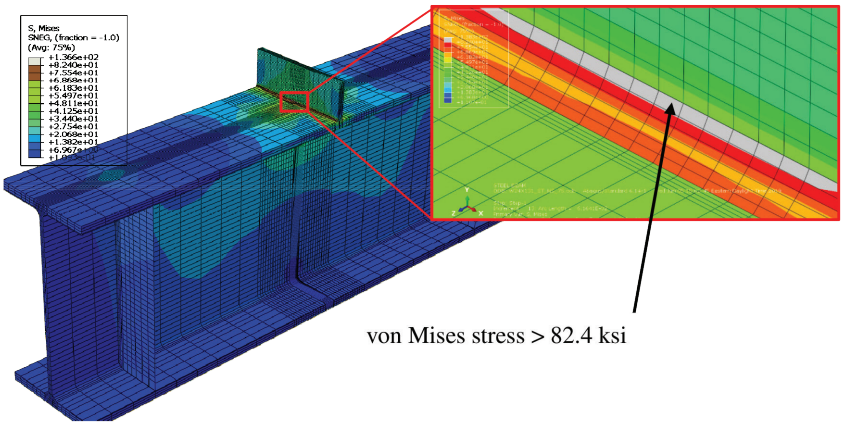

Fig. 16. Stress distribution assumed at "failure" for W24×131 ST-NA-¼.

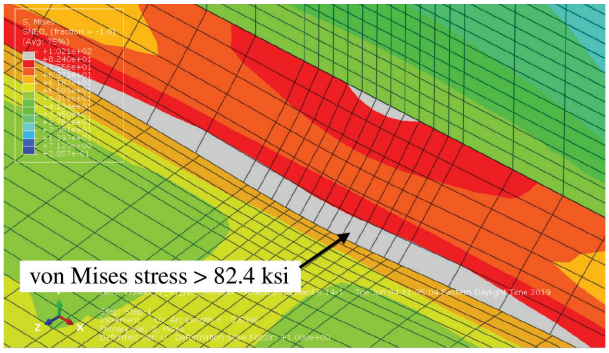

Fig. 17. Stress distribution at assumed "failure" for W24×131 ST-NA-⅞.

increased. Modeling larger sections with smaller weld sizes showed the influence of stiffener eccentricity is minimal because load-carrying capacities are all similar. Figure 18 shows the W24×229 column specimen modeled with ¼-in. welds and no stiffeners and at the assumed failure load. The stresses in the weld are fairly uniform across the width of the column. Analyzing the same column size with concentric stiffeners shows the weld stresses become slightly more uniform, but there is only a small change in the maximum load.

In general, as the column size decreased and the weld size increased, the influence of stiffener eccentricity became more pronounced because the capacity of the models became less governed by limitations in the weld strength itself. Rather, more localized deformations occurred in the flange causing nonuniform weld stresses. As stiffener eccentricity decreased, more uniform stresses occurred in the weld and allowed for achieving a greater capacity.

FINITE ELEMENT MODELS RESULTS AND DISCUSSION

Compression Models – Results and Discussion

Tables 3 and 4 show the theoretical nominal strengths (using AISC equations) and model results as they pertain to (1) achieved load capacity, listed as "maximum load" in the tables; (2) stiffener capacity, listed as "effective stiffener capacity" in the tables; and (3) the percentage of capacity provided by an eccentric stiffener compared to the concentric stiffener case, listed as "% concentric stiffener" (these three parameters are herein noted as "primary results" for single compression models and double compression models, respectively.) Tables 3 and 4 also provide general information for the finite element models, including the column size, the stiffener condition, and the stiffener thickness, *t*. The nominal strengths shown in the tables are for the applicable limit states using the AISC *Specification* (AISC, 2016), which includes web local yielding (WLY); web local crippling (WCR); and for double compression tests, web compression buckling (WCB).

For single compression models shown in Table 3, two larger column sizes, W14×233 and W24×229, were modeled with ¾-in. stiffeners. The double compression model results are only shown when utilizing ¾-in.-thick stiffeners in Table 4. Kowalkowski and Alvarez Rodilla (2019) described models implementing ⅜-in. stiffeners. The results with ⅜-in. stiffeners were inconsistent and did not relate well to the rest of the studies performed for the analytical investigations. Certain models utilizing ⅜-in. stiffeners behaved poorly as elastic buckling occurred in the stiffener before distribution of load into the web. In addition, a ⅜-in. stiffener thickness is small for compression conditions when utilizing AISC *Specification* Section J10.8 (AISC, 2016).

Note that evaluation of the concentrated load limit states in the AISC *Specification* (AISC, 2016) was not a primary focus of the research. However, the results presented in Tables 3 and 4, and for the single tension results shown later, demonstrate significant differences between the computed nominal capacities and the analytical results, and therefore question the accuracy of the equations in the AISC *Specification* (2016), particularly for the limit states of web compression buckling and flange bending.

The results in Table 3 demonstrate that the maximum loads obtained for single compression column specimens without stiffeners are close to the theoretical capacity for web local crippling when column specimens have more

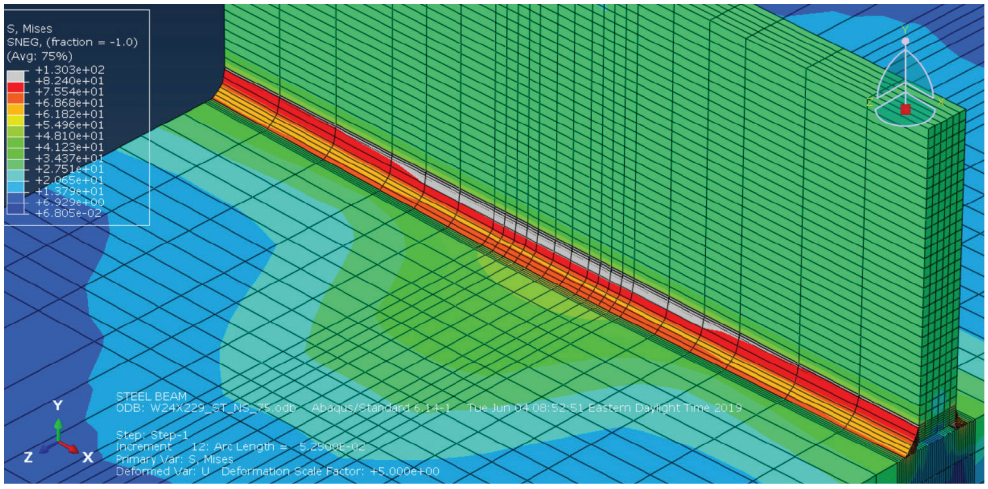

Fig. 18. Single tension model of W24×229 ST-NA-¼ at maximum assumed load.

Table 3. Primary Results for Single Compression Tests							
General Information			Nominal Strengths using 2016 AISC *Specification*		Primary Results		
Column Size	Stiffener Eccentricity (in.)	Stiffener *t* (in.)	WLY (kips)	WCR (kips)	Maximum Load (kips)	Effective Stiffener Capacity (kips)	% Concentric Stiffener
W24×131	NA	⅜	244	465	440	—	—
W24×131	0	⅜			676	236	—
W24×131	2	⅜			559	118	50.2
W24×131	4	⅜			503	62.5	26.5
W24×229	NA	⅜	571	1230	992	—	—
W24×229	0	⅜			1120	130	—
W24×229	2	⅜			1110	115	88.0
W24×229	4	⅜			1060	66.1	50.8
W24×229	NA	¾			992	—	—
W24×229	0	¾			1300	305	—
W24×229	2	¾			1200	210	68.8
W24×229	4	¾			1110	120	39.3
W14×68	NA	⅜	152	234	232	—	—
W14×68	0	⅜			336	104	—
W14×68	2	⅜			275	42.1	40.7
W14×68	4	⅜			235	2.90	2.80
W14×120	NA	⅜	249	456	404	—	—
W14×120	0	⅜			502	97.9	—
W14×120	2	⅜			465	61.0	62.3
W14×120	4	⅜			419	14.8	15.1
W14×176	NA	⅜	428	896	660	—	—
W14×176	0	⅜			754	94.5	—
W14×176	2	⅜			723	64.0	67.7
W14×176	4	⅜			693	33.9	35.9
W14×233	NA	⅜	508	1500	966	—	—
W14×233	0	⅜			1060	91.0	—
W14×233	2	⅜			1030	64.9	71.4
W14×233	4	⅜			1010	42.5	46.7
W14×233	NA	¾			966	—	—
W14×233	0	¾			1230	265	—
W14×233	2	¾			1120	152	57.6
W14×233	4	¾			1030	60.2	22.7

Table 4. Primary Results for Double Compression Tests								
General Info			Nominal Strengths using 2016 AISC *Specification*			Primary Results		
Column Size	Stiffener Eccentricity (in.)	Stiffener *t* (in.)	WLY (kips)	WCR (kips)	WCB (kips)	Maximum Load (kips)	Effective Stiffener Capacity (kips)	% Concentric Stiffener
W24×131	NA	NA	244	465	297	469	—	—
W24×131	0	¾				891	422	—
W24×131	2	¾				877	408	96.7
W24×131	4	¾				601	132	31.3
W24×229	NA	NA	571	1230	1190	1040	—	—
W24×229	0	¾				1480	437	—
W24×229	2	¾				1300	258	59.0
W24×229	4	¾				1290	253	57.8
W14×68	NA	NA	152	234	182	274	—	—
W14×68	0	¾				649	375	—
W14×68	2	¾				461	187	49.9
W14×68	4	¾				287	12.8	3.4
W14×120	NA	NA	249	456	520	476	—	—
W14×120	0	¾				854	378	—
W14×120	2	¾				777	301	79.7
W14×120	4	¾				593	117	31.0
W14×176	NA	NA	428	896	1450	850	—	—
W14×176	0	¾				1220	368	—
W14×176	2	¾				1160	311	84.4
W14×176	4	¾				995	145	39.4
W14×233	NA	NA	508	1500	2830	1280	—	—
W14×233	0	¾				1560	276	—
W14×233	2	¾				1670	388	140
W14×233	4	¾				1480	205	74.1

slender webs (W14×68 and W24×131). However, for the remaining column specimens, the maximum load was found between the theoretical capacities for web local yielding and web local crippling. The results in Table 4 indicate that for double compression specimens without stiffeners and with more slender webs (W14×68 and W24×131), the theoretical capacity for web compression buckling significantly underestimates the maximum load. In contrast, for column specimens with stockier webs (W14×120, W14×176, and W14×233), the capacity for web compression buckling overestimates the maximum load. Failure modes for stockier columns are best described as inelastic web compression buckling as described in Kowalkowski and Alvarez Rodilla (2019).

Comparisons between the maximum load obtained and web compression buckling are quite varied as demonstrated graphically in Figure 19. In Figure 19, CAP represents the maximum load capacity obtained in the finite element model for practical column sizes or experimentally for the sizes tested in the lab. The figure shows bar graphs to represent ratios of the theoretical limit states (WLY, WCB, and WCR) versus the maximum load capacity. Ratios less than 1.0 would indicate that the limit state equations are conservative with respect to design. Despite web compression buckling being the observed mode of failure in all analytical models (from the deformed shape), results in Figure 19 demonstrate that the maximum loads compare well to the limit state of web local crippling (ratio of WCR/CAP

always between 0.8 and 1.2). In addition, the maximum load is always consistently higher than the capacity for web local yielding. However, yielding was identified in all models, resulting in inelastic deformations that may be undesirable in the design of a beam-column joint.

Tables 3 and 4 show that the maximum load capacities for column specimens with stiffeners are always higher than the equivalent condition without stiffeners. However, for specimens with eccentric stiffeners, the "percent of concentric effective stiffener capacity" (shown as "% concentric stiffener" in the table) varies significantly, and the results are highly dependent on column size. As the column size increases, the percent of concentric effective stiffener capacity increases as well. For single compression tests, it was also observed that an increase in stiffener thickness increases the effective stiffener capacity regardless of the column size and the stiffener condition. The percent of concentric stiffener results are higher when ⅜-in. stiffeners are modeled in comparison to when ¾-in. stiffeners are modeled, even though the overall maximum loads obtained when ¾-in. stiffeners are modeled are always higher. Therefore, there are several parameters (various column properties and stiffener thickness) associated with identifying appropriate effective stiffener capacities of eccentric stiffeners. More details regarding the results and findings from the compression tests are provided in Kowalkowski and Alvarez Rodilla (2019).

Single Tension Models—Results and Discussion

All primary results of the single tension tests are provided in Tables 5, 6, and 7 for ¼-in., 9⁄16-in., and ⅞-in. welds, respectively. In the tables, the modified weld capacity for the finite element models assumes a uniform weld stress that can be obtained across the width as described in Kowalkowski and Alvarez Rodilla (2019). The tables show two different results: the "load results," which are equivalent to the results shown for single and double compression, and the "stiffness results," which are described herein. For the load results, the tables list the maximum load interpreted in each analysis (when weld failure is assumed to occur). For all cases with stiffeners, an analytical "effective stiffener capacity" is listed, which represents the difference between the maximum load obtained for that analysis and the result of the corresponding column specimen without stiffeners. The effective stiffener capacities of column specimens with eccentric stiffeners are shown as a percentage of the effective stiffener capacity of the corresponding analysis with concentric stiffeners. The tables show this percentage under the column labeled "% concentric stiffener capacity."

The process for determining when failure occurred in the weld was described earlier. However, the failure load was sensitive to how each increment of the finite element analysis was visually analyzed. Interpreting exactly when failure would occur was still questionable and small errors in this interpretation cause small errors in the primary results of this research. Due to the sensitivity of the results

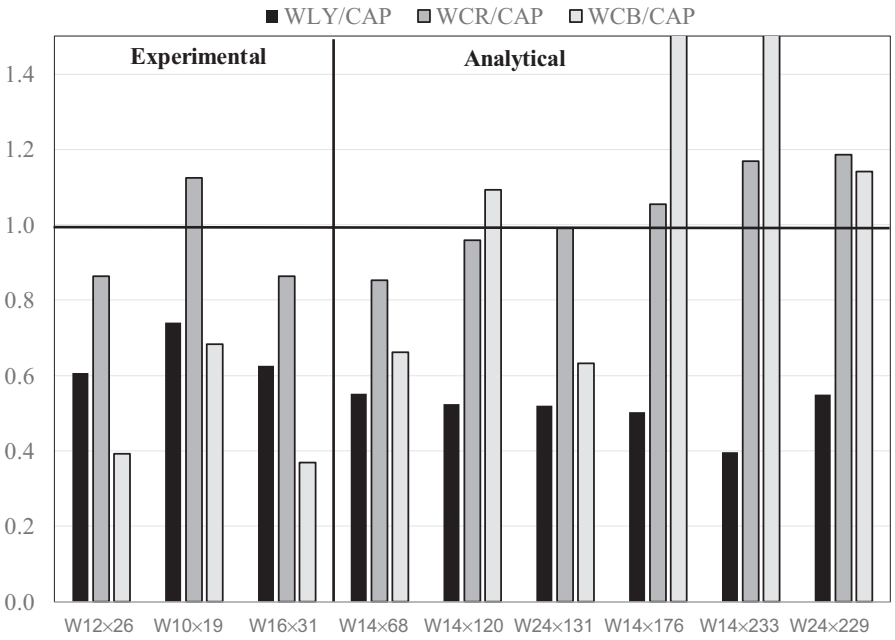

Fig. 19. Ratios of theoretical capacities vs. double compression test capacities.

Table 5. Primary Results of Single Tension Specimens Modeled with ¼-in. Welds								
			Load Results			Stiffness Results		
Column Size	Stiffener Condition	Modified Weld Capacity (kips)	Maximum Load (kips)	Effective Stiffener Capacity (kips)	% Concentric Stiffener Capacity	Stiffness (kips/in.)	Effective Stiffness (kips/in.)	% Concentric Stiffener Stiffness
W24×131	NA	260	216	—	—	4210	—	—
W24×131	E0	260	258	43.0	—	5510	1300	—
W24×131	E2	260	258	42.0	99.0	4900	692	53.3
W24×131	E4	260	235	20.0	47.0	4450	235	18.1
W24×229	NA	264	263	—	—	6800	—	—
W24×229	E0	264	264	0.50	—	7990	1190	—
W24×229	E2	264	263	0.20	30.0	7660	862	72.7
W24×229	E4	264	263	0.10	22.0	7230	426	35.9
W14×68	NA	201	159	—	—	2080	—	—
W14×68	E0	201	200	41.0	—	2320	244	—
W14×68	E2	201	191	31.0	76.0	2180	102	42.0
W14×68	E4	201	169	10.0	24.0	2100	23.0	9.60
W14×120	NA	296	221	—	—	3170	—	—
W14×120	E0	296	295	73.0	—	3610	437	—
W14×120	E2	296	291	69.0	94.0	3410	241	55.0
W14×120	E4	296	253	31.0	43.0	3250	82.0	18.8
W14×176	NA	316	284	—	—	4530	—	—
W14×176	E0	316	316	32.0	—	5110	579	—
W14×176	E2	316	314	31.0	96.0	4920	387	66.7
W14×176	E4	316	312	29.0	90.0	4700	173	29.8
W14×233	NA	320	318	—	—	5980	—	—
W14×233	E0	320	320	1.70	—	6660	682	—
W14×233	E2	320	319	1.50	87.0	6490	506	74.2
W14×233	E4	320	319	1.20	70.0	6240	265	38.9

with respect to the interpreted weld failure (e.g., very small effective stiffener capacities for W24×229 column specimen from Table 5), changes in the elastic stiffness were also evaluated. Herein, the "effective stiffener stiffness" represents the change in elastic stiffness when stiffeners are used in comparison to the elastic stiffness when stiffeners are not used. "Elastic stiffness" represents load divided by the displacement at the top of the loading plate. The displacement at the top of the loading plate considers flexural and shear deformations that occur in the column specimen, elastic elongation of the loading plate, and local deformations that occur in the column specimen from the concentrated load effect. If stiffeners are not present, more local deformations occur in the column specimen directly underneath the load due to the concentrated load effect. If concentric stiffeners are used, the local deformations are minimized, and therefore, a significantly higher elastic stiffness is expected. When eccentric stiffeners are used, the elastic stiffness results are between the corresponding values without stiffeners and concentric stiffeners. Therefore, an impression of how much of the applied load is shared by the stiffeners can be interpreted and compared to the concentric stiffener case.

In Tables 5, 6, and 7, the effective stiffener stiffness of column specimens with eccentric stiffeners is shown as a percentage of the effective stiffener stiffness of the corresponding model with concentric stiffeners. This is shown in the tables under the column labeled "% concentric stiffener

Table 6. Primary Results of Single Tension Specimens Modeled with 9/16-in. Welds								
			Load Results			Stiffness Results		
Column Size	Stiffener Condition	Modified Weld Capacity (kips)	Maximum Load (kips)	Effective Stiffener Capacity (kips)	% Concentric Stiffener Capacity	Stiffness (kips/in.)	Effective Stiffness (kips/in.)	% Concentric Stiffener Stiffness
W24×131	NA	584	402	—	—	5050	—	—
W24×131	E0	584	542	140	—	5980	939	—
W24×131	E2	584	513	111	79.1	5650	604	64.0
W24×131	E4	584	445	42.9	30.7	5270	221	24.0
W24×229	NA	593	590	—	—	8340	—	—
W24×229	E0	593	591	1.30	—	9350	1000	—
W24×229	E2	593	591	0.80	59.3	9110	765	76.0
W24×229	E4	593	590	0.70	50.3	8730	391	39.0
W14×68	NA	453	260	—	—	2260	—	—
W14×68	E0	453	325	65.2	—	2430	171	—
W14×68	E2	453	308	48.9	75.0	2360	102	60.0
W14×68	E4	453	275	15.5	23.7	2290	25.0	15.0
W14×120	NA	666	450	—	—	3500	—	—
W14×120	E0	666	621	172	—	3790	297	—
W14×120	E2	666	562	113	65.7	3700	205	69.0
W14×120	E4	666	485	35.7	20.8	3570	73	25.0
W14×176	NA	711	590	—	—	5050	—	—
W14×176	E0	711	700	109	—	5450	400	—
W14×176	E2	711	686	95.3	87.3	5350	293	73.0
W14×176	E4	711	652	61.8	56.7	5190	132	33.0
W14×233	NA	720	704	—	—	6750	—	—
W14×233	E0	720	717	12.3	—	7220	468	—
W14×233	E2	720	716	11.4	92.7	7120	364	78.0
W14×233	E4	720	715	10.4	84.9	6950	191	40.8

stiffness." As shown in the tables, there are clear trends in the result of percent of concentric stiffener stiffness. As column size increases and eccentricity decreases from 4 in. to 2 in., the percent of concentric stiffener stiffness increases. Therefore, the results of the elastic stiffness and effective elastic stiffness were found as beneficial when studying the effects of stiffener eccentricity as opposed to the maximum load.

The results in Tables 5, 6, and 7 demonstrate that the weld size and loading plate thickness significantly influence load carrying capacity within the model. The failure load always increased when the column size remained constant and only the weld size and loading plate thickness increased. Comparisons between the results and the limit states of flange bending and web local yielding are provided in Kowalkowski and Alvarez Rodilla (2019). The failure load results when using ¼-in. welds were often less than or close to the flange bending capacity and web local yielding capacities. However, incorporating ⅞-in. welds into the models significantly increased the analytical capacity in comparison to the limit state of flange bending and web local yielding. This observation demonstrates that the calculations for web local yielding and flange bending are not "true" capacities. However, weld failure is influenced

Table 7. Primary Results of ST Specimens Modeled with ⅞-in. Welds								
			Load Results			Stiffness Results		
Column Size	Stiffener Condition	Modified Weld Capacity (kips)	Maximum Load (kips)	Effective Stiffener Capacity (kips)	% Concentric Stiffener Capacity	Stiffness (kips/in.)	Effective Stiffness (kips/in.)	% Concentric Stiffener Stiffness
W24×131	NA	908	582	—	—	5470	—	—
W24×131	E0	908	772	190	—	6260	788	—
W24×131	E2	908	742	160	84.0	6130	655	83.0
W24×131	E4	908	666	84.3	44.0	5750	280	36.0
W24×229	NA	923	903	—	—	9040	—	—
W24×229	E0	923	916	12.6	—	9940	897	—
W24×229	E2	923	915	11.7	92.0	9800	766	85.0
W24×229	E4	923	913	9.8	77.0	9480	438	49.0
W14×68	NA	704	348	—	—	2390	—	—
W14×68	E0	704	436	88.1	—	2510	122	—
W14×68	E2	704	431	83.1	94.0	2500	113	93.0
W14×68	E4	704	400	51.6	59.0	2420	36.0	29.0
W14×120	NA	1040	613	—	—	3700	—	—
W14×120	E0	1040	678	65.1	—	3940	241	—
W14×120	E2	1040	674	61.1	94.0	3920	215	89.0
W14×120	E4	1040	661	48.2	74.0	3800	95.0	39.0
W14×176	NA	1110	855	—	—	5330	—	—
W14×176	E0	1110	994	139	—	5680	353	—
W14×176	E2	1110	979	124	89.0	5640	310	88.0
W14×176	E4	1110	930	75.0	54.0	5500	166	47.0
W14×233	NA	1120	1010	—	—	7190	—	—
W14×233	E0	1120	1100	82.6	—	7580	384	—
W14×233	E2	1120	1090	74.6	90.0	7530	338	88.0
W14×233	E4	1120	1060	50.9	62.0	7390	199	52.0

by the effects of flange bending. For instance, if concentric stiffeners are used, flange bending is minimized and higher loads are obtained. In addition, for a group of specimens of the same column size and weld thickness, the lowest failure load always resulted in the specimen without stiffeners, the second lowest in the specimen with stiffeners at a 4-in. eccentricity, the third with stiffeners at a 2-in. eccentricity, and the highest with concentric stiffeners. This research was limited to utilizing fillet welds, but similar trends in the results are expected if the column specimens were loaded with complete joint penetration welds. More research investigations are required to evaluate this assumption.

FORMULATION OF RECOMMENDATIONS BASED ON TEST RESULTS AND FINITE ELEMENT MODELING

Figure 20 represents a comprehensive output of the research to identify appropriate relationships between column section parameters and effective stiffener capacity that are valid or conservative for all test conditions (single tension, single compression, and double compression) and incorporates both experimental and analytical results. As described in Kowalkowski and Alvarez Rodilla (2019), relationships between the percent of concentric stiffener results and several column section properties were evaluated. These column section properties include the flange thickness, the

web slenderness (h/t_w), and the flange slenderness ($b_f/2t_f$). All of these properties contribute to the behavior and subsequent results within the study. However, the most critical and consistent property that influenced the results was the flange thickness, and therefore, final recommendations consider the flange thickness normalized with respect to the magnitude of eccentricity (e).

Figure 20 uses the eccentricity and flange thickness in the form of the e/t_f ratio and plots the results of this ratio versus. either the percent of concentric stiffener results in terms of elastic stiffness (analytical results only) or the percent of concentric stiffener results in terms of maximum capacity. Possible recommended design relationships are also shown in Figure 20. Single tension test results with ¼-in. welds were removed from the data sets in Figure 20 due to limitations of the weld strength, and the percent of concentric stiffener capacity results were sensitive to very small differences in maximum load obtained. Similarly, double compression results with ⅜-in. stiffeners were omitted for reasons described earlier.

Three possible design relationships between the e/t_f ratio and the percent of concentric stiffener results are shown in Figure 20. Data points compared include the experimental results of the study described in Part 1: Experimental Studies (Alvarez Rodilla and Kowalkowski, 2021), and results from the finite element models described in this paper. Three relationships between the data points were examined:

1. A straight-line linear expression, as shown by the gray line.
2. A more conservative parabolic equation (black line) similar to the straight-line equation and providing a maximum allowable e/t_f ratio of 5.0.
3. And the preferred parabolic equation that originates at 100% and provides a maximum e/t_f of 6.0 (red curve).

The third equation is preferred by the authors, but equations are shown for consideration of others to make design decisions. Both parabolic equations indicate that if the eccentricity is 0 in., the effective stiffener capacity is 100% that of the concentric stiffener case and are, therefore, logical. The development of the curves in Figure 20 is based on calibration to the current research. As such, no theoretical basis beyond observed data trends appears in the curves.

Reviewing the results in Figure 20 shows that only one data point falls significantly under the design relationships

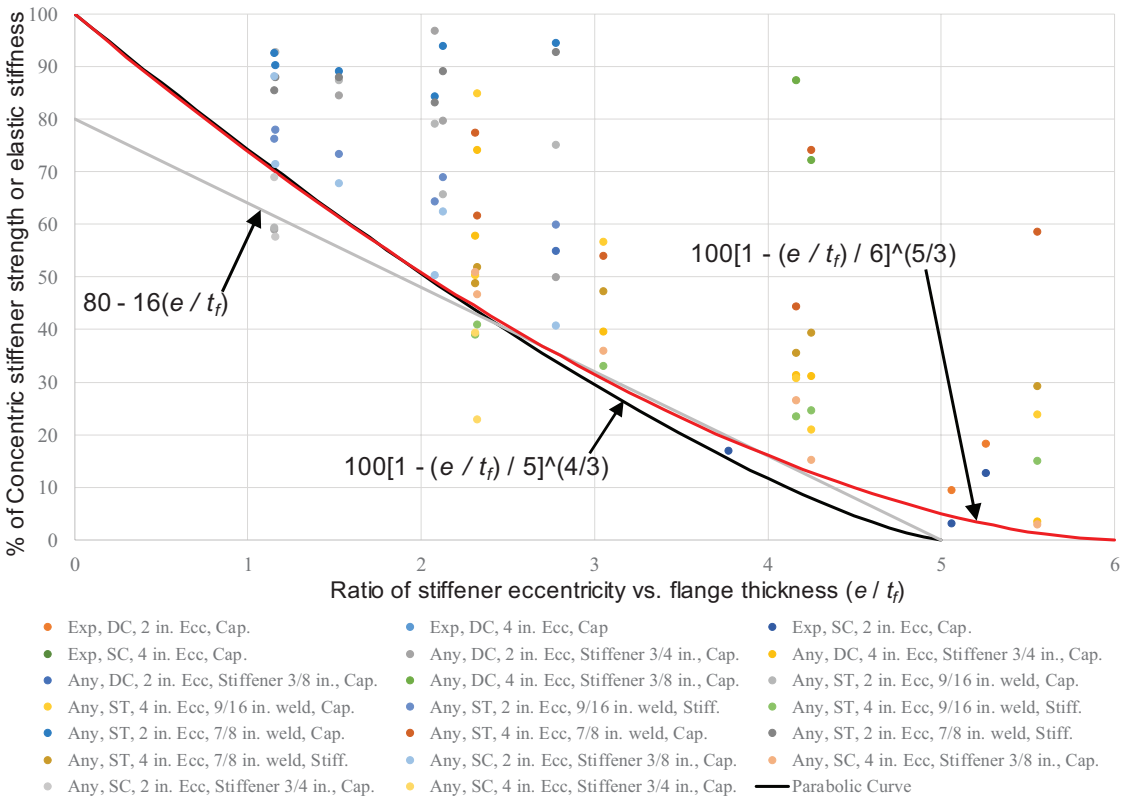

Fig. 20. All data used to define the relationship between e/t_f *and percent of concentric stiffener results.*

(at $e/t_f \approx 2.3$). This data point reflects the result of the analytical single compression test of the W24×229 column specimen modeled with ¾-in. stiffeners at an eccentricity of 4 in. This data point, based on careful review, is interpreted to be an outlier in the data, and all remaining comparisons fall above the recommended design relationships or very close to them.

CONCLUSIONS AND RECOMMENDATIONS

The following are the primary conclusions from the analytical investigations considering single compression, double compression, and single tension test results and the further studies presented in Kowalkowski and Alvarez Rodilla (2019).

- The equations in the AISC *Specification* (AISC, 2016) for the limit state of web local crippling compare favorably to the analytical finite element model results. Meanwhile, the equations for the limit state of web local yielding severely underestimate the capacity of column specimens subjected to concentrated loads.
- The equation for the limit state of web compression buckling is inconsistent compared to the capacity found in the finite element models considering double compression loading, even though this was the mode of failure identified in the finite element models for all column specimens without stiffeners.
- The recommended eccentric capacity calculations included in AISC Design Guide 13 (Carter, 1999) do not appear to properly identify the effective stiffener capacity of eccentric stiffeners for the cases considered in this research.
- This research shows that the effective stiffener capacity of eccentric stiffeners is dependent on several factors, including:
  1. The type of applied loading (single compression, double compression, or single tension).
  2. Column dimensions such as flange and web thickness, slenderness ratios, and overall cross-sectional size.
  3. Weld sizes, with respect to the single tension condition, for the component pulling on the column flange.
  4. Stiffener thickness and magnitude of eccentricity.
- The number of variables are many, but determining the effective stiffener capacity can conservatively be simplified using the flange thickness and magnitude of eccentricity.

From this research, recommendations for computing the final effective stiffener capacity, R_{n_eff}, are provided herein. The capacity assumes that a pair of full-depth transverse stiffeners are provided. Also, the effective stiffener capacity calculated utilizes the preferred parabolic function shown in Figure 20 (red line). The following design recommendations for stiffeners used within moment connections of beams connecting to column flanges are:

- When a column specimen is subjected to a single or double concentrated compression load, it is recommended that stiffeners pass the slenderness limit in Equation 1:

$$\lambda_s = \frac{b_s}{t_s} \le 0.56\sqrt{\frac{E}{F_{ystiff}}} \tag{1}$$

- For the following conditions, based on limitations and observations in this research, eccentric stiffeners shall have no effective stiffener capacity, $R_{n\_eff} = 0$, if any of the following criteria are met:
  - If the eccentricity, e, is greater than 4 in.
  - If the flange thickness, t_f, is less than 0.5 in.
  - If the ratio of e/t_f is greater than 6.0.
- Assuming the preceding conditions do not apply, the effective stiffener capacity of eccentric stiffeners is computed using Equation 2.

$$R_{n\_eff} = R_{n\_c}\left(1 - \frac{e/t_f}{6}\right)^{5/3} \tag{2}$$

where

R_{n_c} = stiffener capacity in the concentric case using acceptable methods, kips

e = actual stiffener eccentricity, in.

LIMITATIONS

The recommendations provided are limited to the largest cross section examined in this research and should be reviewed using additional section sizes and stiffener sizes and depths. Eccentricities greater than 4 in. could be evaluated for larger column sizes. Analysis should be performed with single tension tests, assuming that the loading plates are attached to the column using complete joint penetration welds.

ACKNOWLEDGMENTS

This research was sponsored by the American Institute of Steel Construction (AISC) and conducted using the laboratory facilities of Lawrence Technological University (LTU). The data compilation and report preparation were supported by the Department of Civil and Architectural Engineering and LTU, and all DIC data from Part 1: Experimental

Studies (Alvarez Rodilla and Kowalkowski, 2021) was processed in collaboration to the Department of Mechanical Engineering at LTU.

REFERENCES

ABAQUS (2014), *ABAQUS/Standard User's Manuals*, Version 6.14, Dassault Systems, 2014.

AISC (2017), *Steel Construction Manual*, 15th Ed., American Institute of Steel Construction, Chicago, Ill.

AISC (2016), *Specification for Structural Steel Buildings*, ANSI/AISC 360-16, American Institute of Steel Construction, Chicago, Ill.

Alvarez Rodilla, J. and Kowalkowski, K.J. (2021), "Determination of Capacities of Eccentric Stiffeners Part 1: Experimental Studies," *Engineering Journal*, AISC, Vol. 58, No. 2, pp. 79–98.

ASTM (2009), *Standard Test Methods for Tension Testing of Metallic Materials*, ASTM E8/E8M-09, ASTM International, West Conshohocken, Pa.

Bowman, M.D. and Quinn, B.P. (1994), "Examination of Fillet Weld Strength," *Engineering Journal*, AISC, Vol. 31, pp. 98–108.

Carter, C.J. (1999), *Stiffening of Wide-Flange Columns at Moment Connections: Wind and Seismic Applications*, Design Guide 13, AISC, Chicago, Ill.

Graham, J.D., Sherbourne, A.N., and Khabbaz, R.N. (1959), "Welded Interior Beam-to-Column Connections," Report for AISC, Chicago, Ill.

Kartal, M., Molak, R., Turski, M., Gungor, S., Fitzpatrick, M.E., and Edwards, L. (2007), "Determination of Weld Metal Mechanical Properties Utilizing Novel Tensile Testing Methods," *Applied Mechanics and Materials*, Vols. 7–8, pp. 127–132.

Kowalkowski, K.J. and Alvarez Rodilla, J. (2019), "Analysis and Design of Eccentric Stiffeners Part of Moment Connections to Column Flanges," Final Report for AISC, Chicago, Ill.

Norwood, J. (2018), "Effect of Continuity Plate Eccentricity on the Performance of Welded Beam-to-Column Connections," Master's Thesis, Department of Civil Engineering, University of Arkansas, Fayetteville, Ark.

Sherbourne, A.N. and Murthy, D.N.S. (1978), "Computer Simulation of Column Webs in Structural Steel Connections," *Computers and Structures*, Vol. 8., May, pp. 479–490.